

The WARP Reactor Concept

M. G. Anderson¹, J. K. Walters¹, E. M. Anaya¹, D. A. Max², W. A. Stygar¹ and A. J. Link¹

¹Lawrence Livermore National Laboratory, Livermore, California 94550, USA

²Mission Support and Test Services, Livermore, California 94550, USA

(Dated: 08 June 2023)

The WARP Reactor Concept promises orders of magnitude increase of intense ion beam energies and respective radiation yields at a fraction of the size and cost over existing z-pinch class accelerators allowing the economically viable study of new Relativistic High Energy Density Physics regimes for probing the intersection between General Relativity and Quantum Field Theory along with game-changing direct applications from rep-rated Magnetized Liner Inertial Fusion devices for energy production and advanced propulsion to multi-pulse compact flash x-ray/neutron radiography sources for assessing our Nation's aging nuclear weapons stockpile. An overview of the WARP Reactor Concept is presented.

Keywords— warp reactor, particle accelerator, dense plasma focus, z-pinch, relativistic high energy density physics, quantum gravity, magnetized liner inertial fusion, advanced propulsion, compact flash x-ray and neutron source radiography

I. INTRODUCTION

The Wave Accelerated Ring Pinch or “WARP” Reactor [1,2] (patent pending), iso-view shown in Figure 1, is expected to solve key issues ranging from our present energy dependence on finite fossil fuels and its associated climate impact to our aging nuclear weapons stockpile. The WARP Reactor promises orders of magnitude increase of ultra-intense ion beam energies and respective high radiation yields at a fraction of the size and cost over other z-pinch class accelerators [3-5] allowing the economically viable and environmental friendly study of new Relativistic High Energy Density (RHED) Physics regimes for probing the intersection between General Relativity and Quantum Field Theory (i.e. Warp/Unruh/Casimir effects) [6-24] along with game-changing direct applications from rep-rated Magnetized Liner Inertial Fusion (MagLIF) devices for energy production and advanced propulsion to multi-pulse compact flash x-ray/neutron radiography sources [3-5,25] for assessing our Nation's aging nuclear weapons stockpile.

II. NOVELTY

The WARP Reactor concept is a novel, modular and compact pulsed power-driven radiation source intended for nuclear fusion energy production, advanced propulsion, accessing new RHED physics regimes and flash radiography/interrogation techniques. WARP utilizes state-of-the-art pulsed power modules to drive its “WARP Core” which consists primarily of two Dense Plasma Focuses (DPFs) [26,27] and two Ion Ring Marx Generators (IRMGs) fired directly at one another. The WARP Reactor's dramatic performance boost is achieved with the use of a novel WARP Core which injects two tubular dense plasma and ion beams from opposite ends of a

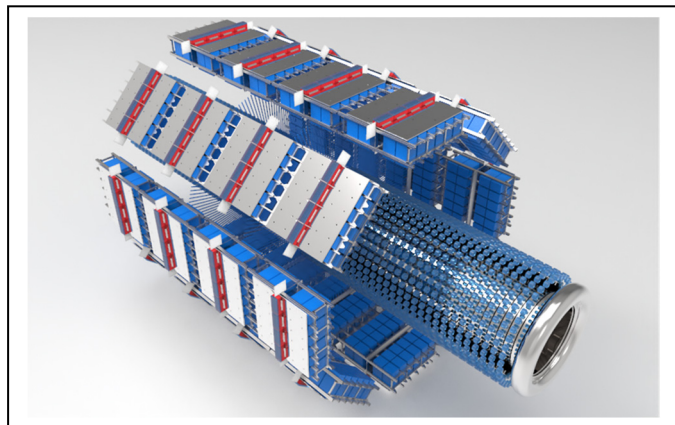


Fig. 1. Iso-view of The WARP Reactor

double-barreled DPF head with embedded IRMG-driven reflex triodes [28] and through magnetic cusps into an axial seed B-field to form co-rotating ion rings which merge near the mid-plane of the device and are subsequently radially compressed and azimuthally accelerated up to 1000 times the initial ion beam energies during the axial magnetic flux compression phase driven by the DPF plasma liner implosion. Two DPF and IRMG heads are implemented to dramatically reduce the size and cost of the drivers and increase ion ring capture efficiency along with the added benefits of favorable magnetic field line curvature throughout implosion process due to higher velocity shear-stabilized DPF plasma pinch flows near each gun muzzle and greater tuning capability for properly timing the implosion and ion beam generation, injection and compression of the two colliding and subsequently merged ion rings onto a solid or high energy density plasma target.

III. STRATEGIC IMPORTANCE

WARP directly aligns with the DOE and NNSA missions and core competencies as an economically viable and climate-friendly rep-rated MagLIF device for nuclear fusion energy production as well as a multi-pulse compact flash x-ray/neutron source for assessing our aging nuclear weapons stockpile. In addition to developing the next-generation pulsed power architectures, this Strategic Initiative will help to benchmark present high-performance computing, simulation, and data science with respect to more disruptive and imaginative ultra-intense plasma/beam configurations. Finally, WARP success would fortify LLNL's place at the forefront of the subsequent RHED physics and technology revolution.

IV. WARP REACTOR PHYSICS

The WARP Reactor conceptual design, models, simulations, and targeted performance characteristics for the various applications pull directly from standard fusion plasma, beam, accelerator and relativistic physics along with a modified Einstein Field Equation (EFE) [29] and respective Figures Of Merit (FOM) for assessing the validity of a recently proposed Naïve Quantum Gravity (NQG) theory [30].

A. Ring Pinch and Acceleration Physics

The physics behind charged particle ring radial compression and azimuthal acceleration [31-40] in the WARP Core is as follows: Magnetic flux (Φ_z) compression (i.e. conservation of seed Φ_z during DPF z-pinch driven imploding liners: $\Phi_z = B_z \pi r^2 = \text{constant}$) creates a "Magnetic Wave" (i.e. seed B_z amplitude rapidly swells/increases since flux conservation dictates that $B_z \propto r^{-2}$) which forces (i.e. $F = qV \times B$) charged particle rings to radially compress (i.e. decrease in Larmor radius: $r_L = \gamma m V_\theta / qB$) and due to the conservation of canonical angular momentum (i.e. $p_\theta = \gamma m r V_\theta + q \Phi_z / 2\pi = \text{constant}$) and adiabatic flux conservation condition (i.e. $p_\theta^2 / B_z = \text{constant}$ or $p_\theta r = \text{constant}$) the charged particle ring azimuthal velocities scale as: $V_\theta \propto (r_i / r_f)$ for $\gamma = 1$. Since Φ_z and p_θ are conserved in this device, final charged particle ring energy is: $E_f = \frac{1}{2} \gamma N m (V_\theta)^2 \sim E_i (r_i / r_f)^2$. Finally, for relativistic charged particle motion in pulsed B-fields, γ varies due to $\nabla \times \mathbf{E} = -(\delta \mathbf{B} / \delta t)$ and therefore $E_f \sim E_i (B_f / B_i)$.

B. Fusion Plasma Physics

The principal formulas used in the WARP Reactor conceptual models and simulations are the standard fusion plasma physics [41-45] equations in MKS units unless specifically identified otherwise (1)-(11) for: N_n – the number of fusion-generated neutrons; β – plasma to magnetic pressure; E_f – total fusion energy; E_p – plasma energy; E_b – bremsstrahlung and E_s – synchrotron radiation energy; G_s – scientific and G_E – engineering gains; E_{sale} – fusion energy for sale; v_A – Alfvén velocity; τ_R – magnetic reconnection time scales along with plasma and particle beam propagation modes (i.e. $\beta > 1$ for diamagnetic drift mode; $\beta \ll 1$ for collective mode; $\beta \ll 1$ with polarization E-field shorted for single particle mode).

$$N_n \sim n^2 < \sigma v > V \tau \quad (1)$$

$$\beta = \frac{n k T}{B^2 / 2 \mu_0} \quad (2)$$

$$E_f = N_n E_r \quad (3)$$

$$E_p = \frac{3}{2} n V k T \quad (4)$$

$$E_b \sim 10^{-38} Z^2 n^2 T [eV]^{0.5} V \tau \quad (5)$$

$$E_s \sim \frac{2 K q^2 \gamma^4 c}{3 r^2} N_e \tau \quad (6)$$

$$G_s = \frac{E_f}{E_p} \quad (7)$$

$$G_E = \frac{E_f}{E_T} \quad (8)$$

$$E_{sale} = f [E_f - E_p - E_b - E_s] \quad (9)$$

$$v_A = \frac{B}{\sqrt{\mu_0 \rho}} \quad (10)$$

$$\tau_R = \frac{L^2}{\delta v_A} \quad (11)$$

Where n is the plasma density; $< \sigma v >$ is the fusion reaction rate; V is the plasma/beam/ring volume; τ is the confinement time; k is the Boltzmann constant; T is plasma temperature; B is the magnetic field; μ_0 is the vacuum permeability; E_r is the fusion energy per reaction; Z is the atomic number; K is the Coulomb constant; q is the charge; γ is the Lorentz factor; c is the speed of light in vacuum; N_e is the number of electrons; E_T is the total stored energy of reactor; f is the conversion efficiency; ρ is the mass density; L is the half-length of current sheet; and δ is the current sheet half-thickness.

C. Relativistic Formulas, Modified EFE, NQG and FOM

In addition to the standard relativistic formulas for the Lorentz factor (12), momentum (13) and energy (14), we also introduce a modified EFE (15) with a NQG addition (16) that may be accessible by the WARP Reactor for verification or invalidation of the theory along with relevant FOM such as spacetime curvature (17), gravitational potential (18) and frame-dragging effects (19).

$$\gamma = \frac{1}{\sqrt{1 - \frac{v^2}{c^2}}} \quad (12)$$

$$\vec{p} = \gamma m \vec{v} \quad (13)$$

$$E = \gamma m c^2 \quad (14)$$

$$G_{\mu\nu} = \frac{8\pi G}{c^4} (S + A) T_{\mu\nu} \quad (15)$$

$$T_{\mu\nu} \rightarrow \text{Re} \left[\frac{\Psi_f^* \hat{T}_{\mu\nu} \Psi_i}{\langle f | i \rangle} \right] \quad (16)$$

$$C_{\alpha\sigma} = (S + A) \frac{G M}{c^2 V} \quad (17)$$

$$\Phi_{\alpha\sigma} = (S + A) \frac{G M}{c^2 R} \quad (18)$$

$$\Omega_{\alpha\sigma} = (S + A) \frac{G I \omega}{c^2 R^3} \quad (19)$$

$G_{\mu\nu}$ - Einstein curvature tensor; $T_{\mu\nu}$ - energy-momentum tensor; $8\pi G/c^4$ - energy-momentum to curvature coupling constant in vacuum; G - Newton's gravitational constant; "S" - Sarfatti plasma metamaterial effects; "A" - Anderson Unruh/Casimir threshold effects; $T_{\mu\nu}$ - Sutherland NQG addition; $\hat{T}_{\mu\nu}$ - energy-momentum operator; ψ_i and ψ_f^* - initial and final conjugate wavefunctions, respectively; $\langle f | i \rangle$ - final and initial boundary conditions; FOM: $C_{\alpha\sigma}$ - spacetime curvature; $\Phi_{\alpha\sigma}$ - gravitational potential and $\Omega_{\alpha\sigma}$ - frame-dragging effect; M - ring mass; R - ring radius; I - ring moment of inertia; ω - ring angular velocity.

V. WARP REACTOR TECHNOLOGY

The WARP Reactor utilizes tried-and-true Shiva Star-like "TEMPEST" Marx Modules to drive its dual Dense Plasma Focus head and state-of-the-art Impedance-matched Marx Generators (or Linear Transformer Drivers for rapid rep-rate operation) to drive the dual charged particle beam-ring reflex triodes. Figures 2, 3 and 4 show a side-view end-view and cross-sectional view of the full-scale WARP Reactor, respectively. The WARP Reactor consists primarily of 40 TEMPEST modules, 2 Ion Ring Marx Generators and the central WARP Core.

A. TEMPEST Marx Modules

Forty TEMPEST Marx modules drive the dual DPF heads. A cross-sectional view of a single TEMPEST Marx module is provided in Figure 5 which consists of a more robust version of the Shiva Star design with upgraded 1.2MA railgap switches, a seismically-rated welded frame capacitor assembly along with a modified HV output header for the flexible high current coaxial cable connections. Each TEMPEST Module is primarily comprised of four super-duty railgap switches, aluminum parallel plate transmission lines and twenty-four +/-60kV, 250kA high energy density capacitors with a total energy stored per module of ~260kJ and a total 40 module TEMPEST system storage of >10MJ and capable of delivering ~60MA to the DPF loads.

B. Ion Ring Marx Generators

Two IRMGs drive the dual Reflex Triode heads. For single pulse operation, each IRMG is a 30-stage Impedance-matched Marx Generator (IMG) [50] on steroids or a Linear Transformer Driver (LTD) [51] for rapid rate-rate operation. The IMG-version, cross-sectional view shown in Figure 6, consists primarily of 30 segmented coaxial return spools, a continuous tapered inner HV stalk, corona toroid, and 40 bricks per stage with each brick being comprised of two capacitors and a high-performance spark-gap switch. Each IRMG can produce a 1MV,

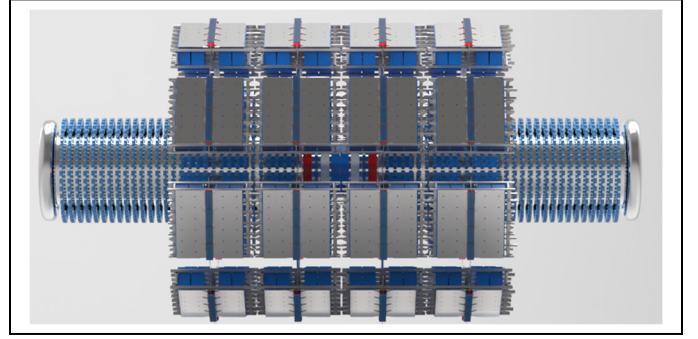


Fig. 2. Side-view of The WARP Reactor (total machine length ~ 18m)

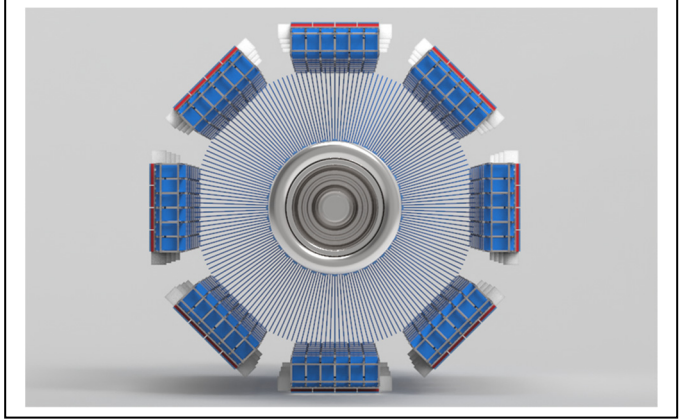


Fig. 3. End-view of The WARP Reactor (total machine diameter: ~ 9m)

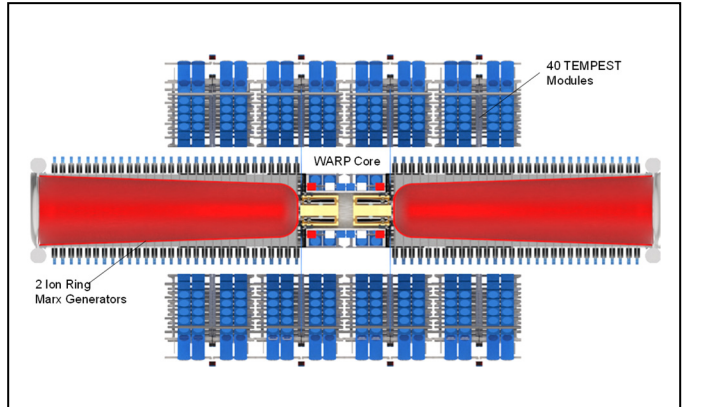


Fig. 4. Cross-sectional view of The WARP Reactor showing TEMPEST Modules, IRMGs and WARP Core

1MA, 100ns pulse to the Reflex Triode with a total energy storage for a two-IRMG system of ~2MJ.

C. WARP Core

Depicted in Figure 7 is a cross-sectional view of the novel WARP Core (~1m L end-to-end x ~0.5m diameter at B-magnets). The relatively large Red, White and Blue squares situated around the grounded vacuum chamber represent the B-insulation, B-Seed and B-cusp pulsed magnets. Whereas the small blue squares (next to the magnets) and internal light blue rectangles are the annular DPF and IRMG puff valves, respectively. The TEMPEST Modules attach to the WARP Core at the DPF Collection Plates on the Left and Right End of the Device. Whereas the Ion Ring Marx Generators connect to the

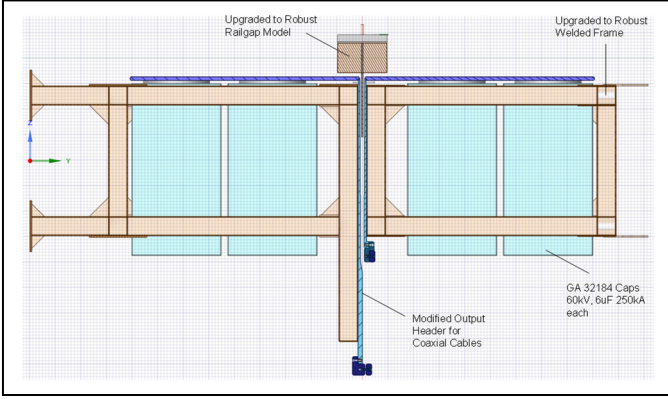


Fig. 5. Cross-sectional view of TEMPEST Marx Module

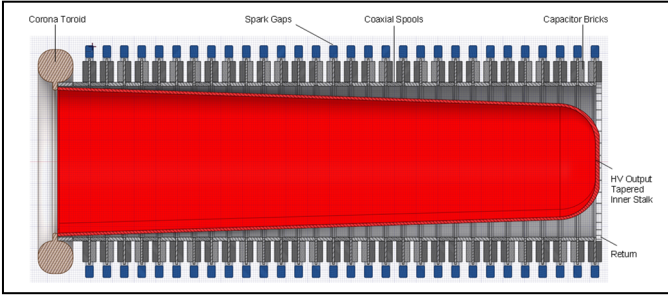


Fig. 6. Cross-sectional view of Ion Ring Marx Generator (IMG-version)

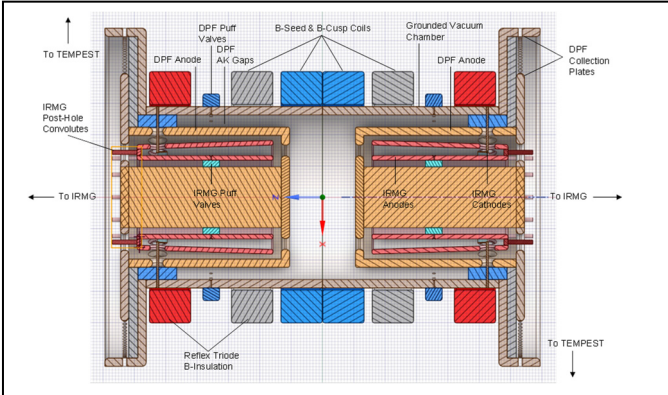


Fig. 7. Cross-sectional view of the WARP Core

two back-ends of the dual Reflex Triodes through the IRMG Post-hole convolutes. Finally, the primary WARP Core and most novel central components consist of coaxial dual DPF (~13cm diameter) and IRMG heads with embedded Reflex Triodes (~10cm diameter).

VI. WARP REACTOR MACHINE METRICS

Table I shows the major pulsed power parameters and DPF plasma liner and Ion Beam/Ring metrics, respectively, along with order of magnitude comparisons with one of the largest ion beam accelerators in recent times, PBFA II. The WARP-X prototype is a 1/10-scale version of the full-scale Reactor which can deliver up to 5MA in < 3us into the DPF plasma liner whereas the 4-stage prototype version of the Ion Ring Marx Generators can generate initial ion beam energies and currents of up to 400keV with 200kA, respectively. The lower section of

TABLE I. WARP REACTOR MACHINE METRICS

WARP-X (1/10 scale of Full Reactor):	4 TEMPEST Modules	2 IRMGs
Capacitor Specs	60kV,6uF,250kA	100kV,160nF,70kA
Total # of Caps	96	64
Railgap Model/Specs	120kV, 1.2MA, 10C	100kV, 120kA, 0.3C
Total Capacitance	144uF erected	160nF erected
Rated Voltage Reversal	60%	20%
Total # of Switches	16	32
Max Vcharge	+/-60kV	+/-50kV
Total Estored	1.04MJ	13kJ
Peak Vout	100kV	400kV
Peak Iout	5MA	400kA
Current Pulse Rise-time / Duration	2.5us	100ns
Rep-Rate	1 shot/15 min	
WARP-X Dimensions	20ft OD x 15ft H	

MACHINE Metrics & Comparisons:	PBFA II / Z	WARP-X	WARP-Reactor	WARP-R/PBFA II
DPF/Z-Pinch Current	NA / 26MA	5MA	60MA	2.3x
Initial Ion Beam/Ring Current	1MA	0.2MA	2MA	2x
Final Ion Beam/Ring Current	1MA	2MA	20MA	20x
Initial Ion Beam/Ring Energy	9MeV	0.4MeV	1MeV	0.11x
Final Ion Beam/Ring Energy	9MeV	40MeV	1GeV	111x
Accel. Efficiency = E_{beam}/E_{stored}	0.66%	15%	25%	38x
Machine Size	108ft ODx16ft H	20ft ODx15ft H	30ft ODx55ft H	0.96x
Total Cost Today	\$250M	\$6M	\$150M	0.6x

Table I provides a comparison of plasma liner/beam/ion ring parameters between PBFA II/Z [52,53] and WARP devices with the 60MA WARP-R (Reactor) machine showing order of magnitude increases in ion beam energy (GeV-level) and current (20MA at implosion stagnation) with 25% acceleration efficiencies.

VII. WARP REACTOR OPERATIONS

Shown in Figures 8-12 are cross-sections of the WARP Core at different phases during operations: PHASE 1 begins with the creation of the B-insulation, B-seed and B-cusp magnetic fields to ensure full B-field diffusion through the metal structures along with gas injection via the DPF and IRMG annular puff valves and subsequent firing of the TEMPEST modules to initiate dual DPF plasmoid generation, lift-off and run-down. PHASE 2 occurs as the two DPFs begin their run-in sequence and the IRMGs are fired to produce the dual tubular ion beams. PHASE 3 is when the DPFs return currents have merged and the dual axially directed ion beams have passed through their respective B-cusp fields to become co-rotating and merged ion rings in the embedded B-seed field. PHASE 4 is the DPF plasma liner implosion sequence which provide the necessary flux compression and subsequent ion ring pinch and azimuthal acceleration. PHASE 5 is the implosion stagnation phase and relativistic high energy density ion ring and target interaction sequence for fusion energy production, advanced propulsion, super-flash x-ray and neutron generation for radiographic and/or

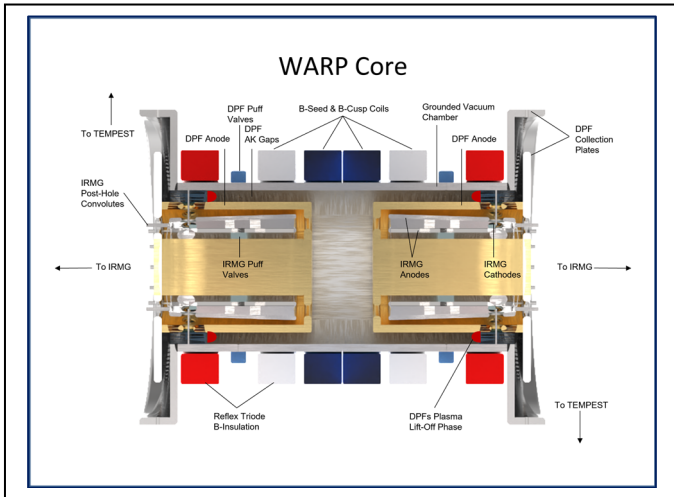


Fig. 8. WARP Reactor Operations: PHASE 1

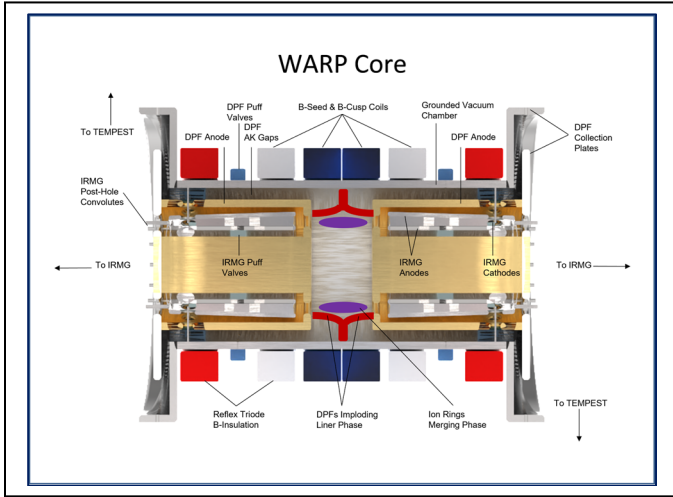


Fig. 11. WARP Reactor Operations: PHASE 4

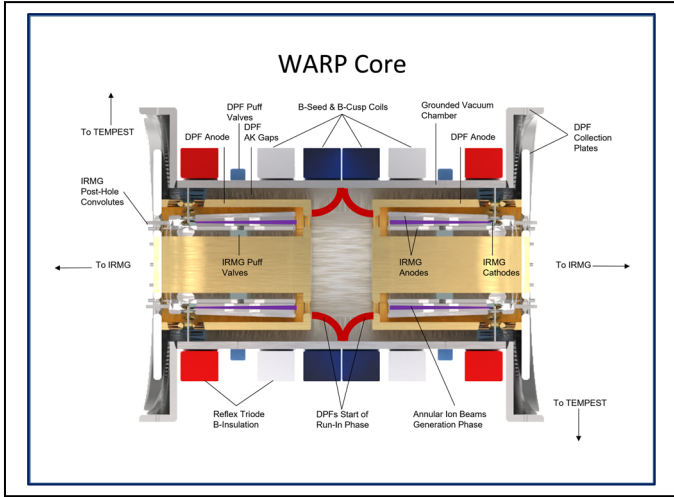


Fig. 9. WARP Reactor Operations: PHASE 2

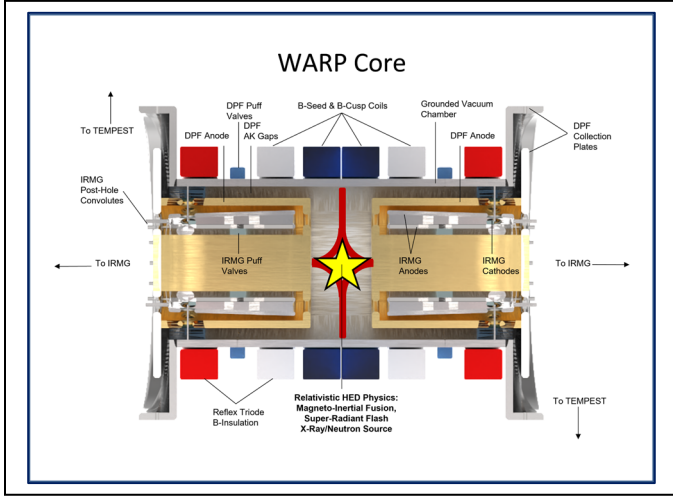


Fig. 12. WARP Reactor Operations: PHASE 5

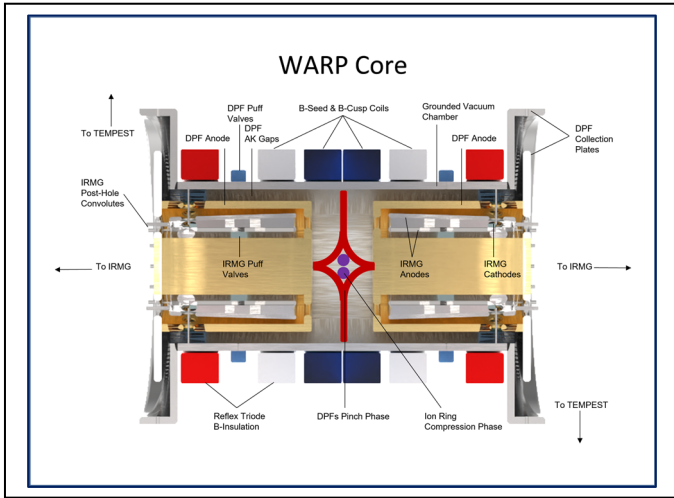


Fig. 10. WARP Reactor Operations: PHASE 3

dynamic interrogation applications and/or accessing new RHED physics regimes.

To aid in visualizing the WARP Core Operations we have created a movie with respective phases identified. [Figures 13-17](#) show the movie's progression from FRAME 1: the DPF plasma lift-off and run-down phases followed by FRAME 2: the Ion Beams Generation and DPF run-in phases then FRAME 3: the Ion Rings Generation and Merging phases followed by FRAME 4: the DPFs and Ion Ring Implosion and Acceleration phases and finally FRAME 5: the WARP Fusion phase, respectively.

VIII. WARP REACTOR MODELS AND SIMULATIONS

To help benchmark our WARP Reactor's plasma liner implosion simulations we compare them to the Semi-Analytical Model for Magnetized Liner Inertial Fusion [54,55], outlined by Dr. McBride from University of Michigan and Dr. Slutz from Sandia, which can be used to reproduce the general 1D behavior of MagLIF machines [3-5]. This model provides many key aspects of MagLIF, including: (1) fuel preheat; (2) liner implosion; (3) liner compressibility, internal magnetic pressure,

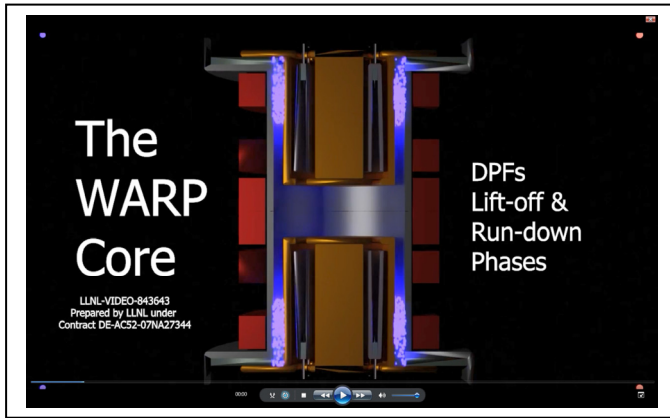


Fig. 13. WARP Reactor Movie Frame 1

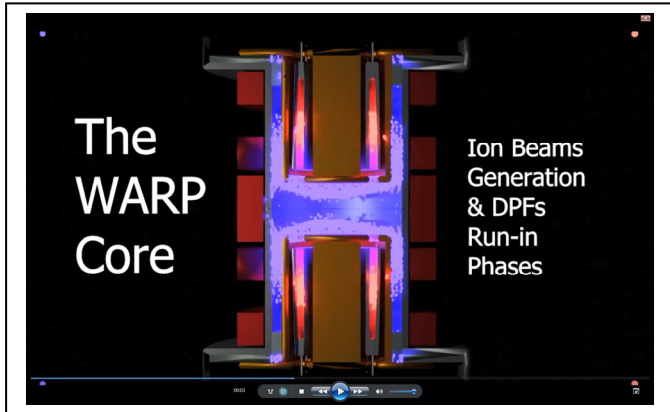


Fig. 14. WARP Reactor Movie Frame 2

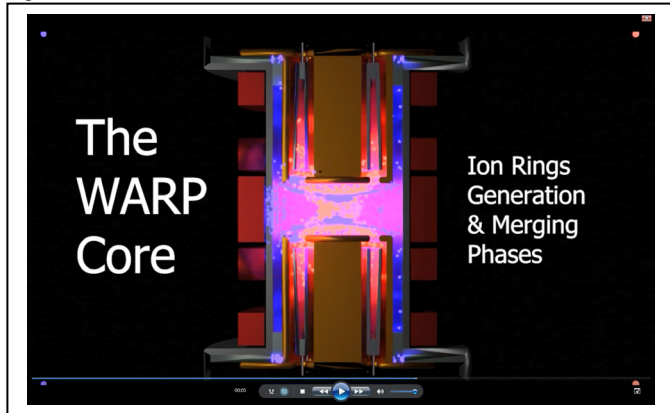


Fig. 15. WARP Reactor Movie Frame 3

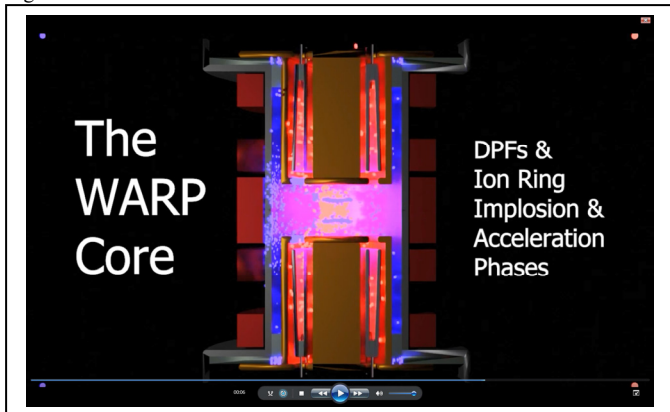


Fig. 16. WARP Reactor Movie Frame 4

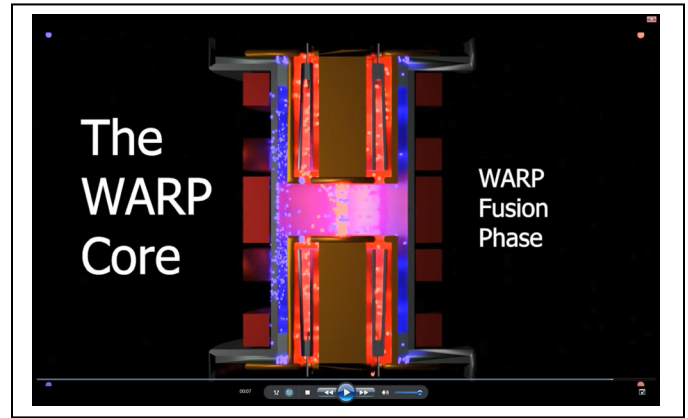


Fig. 17. WARP Reactor Movie Frame 5

and ohmic heating; (4) adiabatic heating by compression; (5) fuel opacity and radiative loss; (6) B-flux compression with; (7) magnetized electron and ion thermal conduction losses; (8) end losses; (9) enhanced losses due to mixing; (10) D-D and D-T primary fusion reactions for fuel ratios; and (11) α -particle fuel heating. However, in order to expedite comparisons between our multi-physics models/simulations and semi-analytical models, we have created a simplified version of their MagLIF model in Mathematica which also allows rapid scanning of WARP Reactor input parameter space for obtaining desired operation scenarios and higher performance regimes.

In addition to the multi-physics models and simulations we of course have created 3D Computer Aided Design (CAD) engineering models with associated Finite Element Analysis (FEA) for electrical and mechanical stresses along with circuit models and simulations for the TEMPEST system, IRMGs (both for single-pulse IMG and rep-rated LTD varieties) and WARP Core dynamic loads, as shown in [Figures 18 and 19](#), respectively.

Unfortunately, due to budget and computational constraints, a somewhat reduced simulation effort was performed for a mini-WARP Core in the Chicago particle-in-cell code in hybrid-kinetic mode where the electrons are treated as an inertia-less fluid using MHD equations for the electron response while the ions are treated as kinetic particles. [Figure 20](#) is a graph of the R-Btheta (or radially enclosed current) and a graph of the respective plasma density at a specific time and both as a function of radial and axial position in centimeters. [Figures 21-25](#) are snapshots of the simulation for the various phases from the dual DPF initial plasma generation, run-down, run-in to the merging and final implosion/pinch phases.

A. DPF Plasmoids Magnetic Reconnection

[Table II](#) captures the magnetic reconnection [56-57] time scales with respect to the DPF plasmoids characteristics as they propagate through their respective B-Cusp regions and just prior to their collision with one another at the midplane of the WARP Core.

B. DPF & Ion Beam Propagation Mechanisms

References [58-63] provide detailed propagation criteria for plasma/beam transport across magnetic field lines in vacuum or within a background magnetized plasma. [Table III](#) captures the

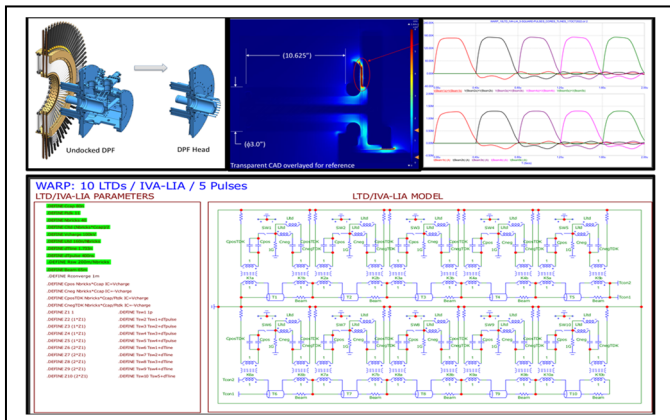


Fig. 18. WARP Reactor CAD modeling, FEA simulations, circuit models and analysis for multi-pulse IRMG (LTD-version) operations

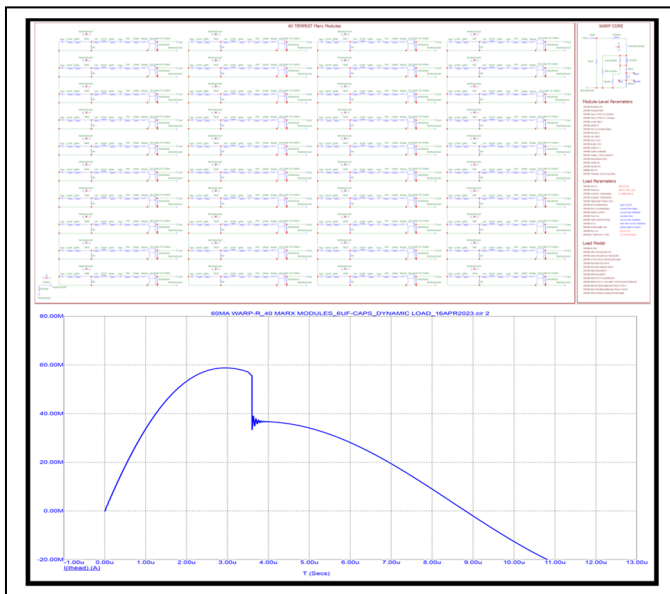


Fig. 19. 60MA WARP Reactor circuit model and analysis for 40 TEMPEST modules driving the WARP Core dynamic load

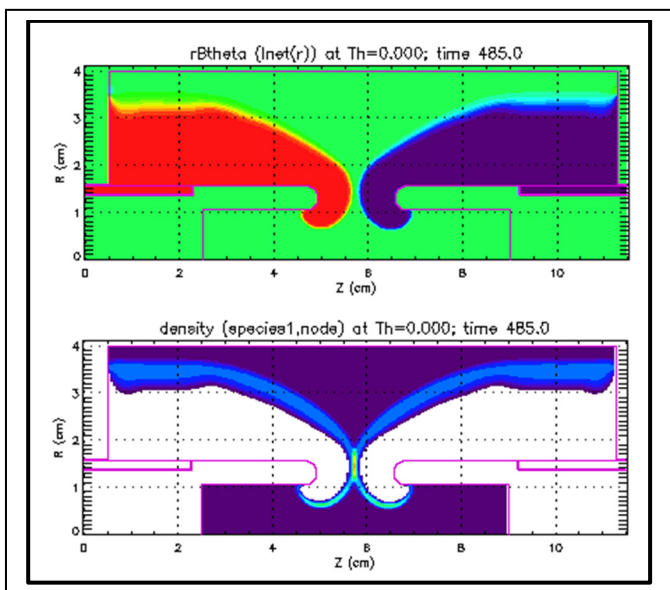


Fig. 20. Mini-WARP Core R-Btheta (top) and plasma density (bottom)

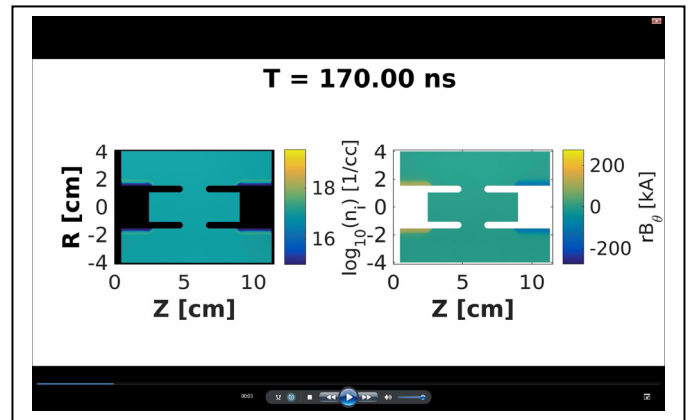


Fig. 21. Mini-WARP Core dual-DPF plasma generation phase

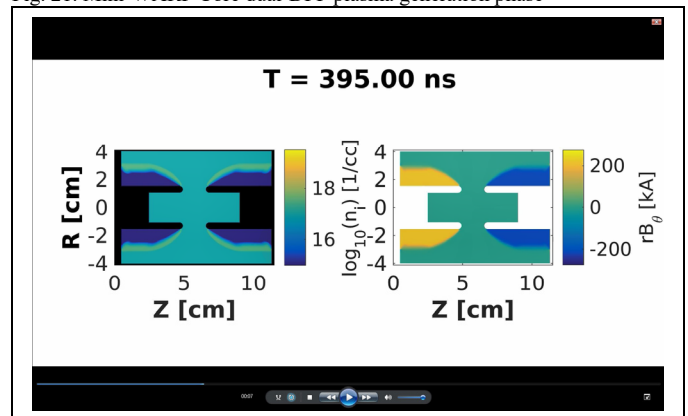


Fig. 22. Mini-WARP Core dual-DPF plasma run-down phase

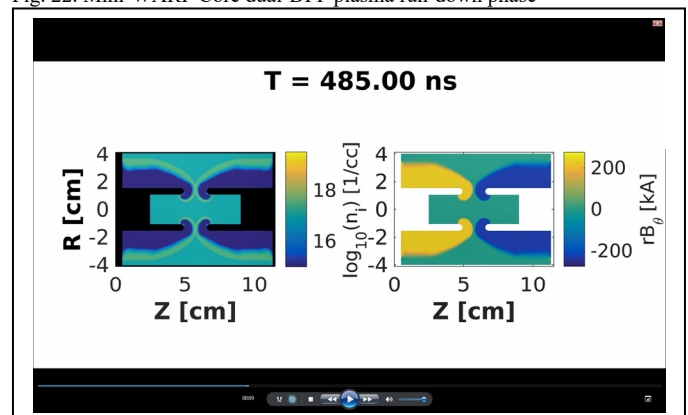


Fig. 23. Mini-WARP Core dual-DPF plasma run-in phase

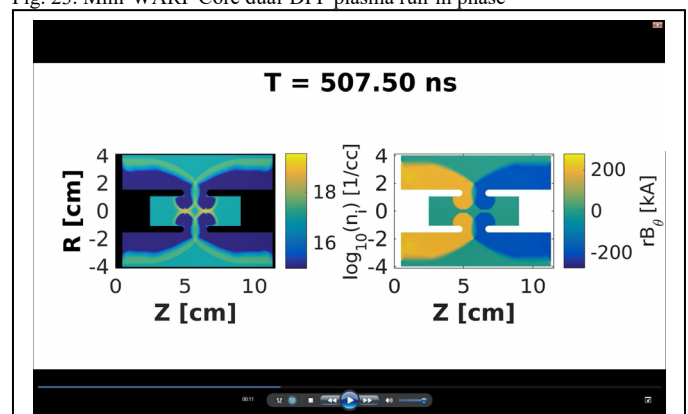


Fig. 24. Mini-WARP Core dual-DPF plasma merging phase

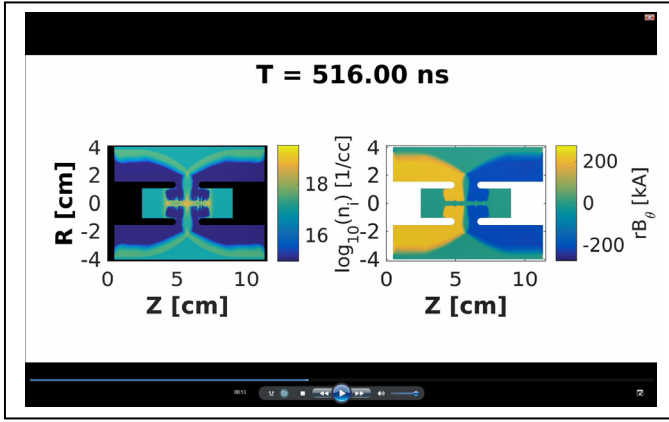


Fig. 25. Mini-WARP Core dual-DPF final implosion and pinch phases

DPF plasmoid initial characteristics and propagation mode via the diamagnetic drift mechanism for this parameter regime. Table IV shows the ion beam propagates in the collective mode unless the polarization E-field is shorted by background electrons. Finally, Table V displays the Reflex Triode and initial ion beam parameters along with final compression (millimeters scale) and accelerations ($>10^{19}$ m/s²). NOTE: of particular interest to Warp, Unruh, dynamic Casimir and QG effects, the electron ring mode of operation indicates submicron implosion radii and $>10^{23}$ m/s² azimuthal accelerations depending on initial e-beam and magnetic flux parameters.

C. Compression, Acceleration, Fusion & Radiation Metrics

Table VI captures the major ring compression and acceleration metrics while Table VII display the overall fusion and radiation metrics for DT operations, respectively. Finally, ion ring major radius at final implosion stagnation reaches the millimeters scale and at GeV-level azimuthal energies for protons, deuterons and tritons. With respect to the fusion/radiation parameters, the peak x-ray and DT fusion neutron yield reach 3.5MJ and 6.6×10^{18} neutrons per pulse, respectively, with an overall scientific gain of >19 .

D. RHED Physics & Metric Engineering

In addition to the fusion energy and x-ray/neutron radiation applications, The WARP Reactor is also primed for accessing new RHED. The 60MA DPF plasma liner with embedded GeV-level ion ring appears capable of reaching thousands of Tesla and subsequently multi-TPa pressures as captured in Table VIII. Due to the dramatic compression and acceleration of the charged particle rings and plasma liner/target interactions we may even begin to generate significant plasma metamaterial, Warp, Unruh and Dynamic Casimir effects not to mention copious amounts of synchrotron radiation from electron ring modes of operations. Furthermore, once the charged particle rings become relativistic during the final moments of implosion phase the decrease in ring radius saturates as relativistic mass increases. In other words, flux compression shifts from ring velocity to ring mass or enhanced spacetime coupling. Finally, the WARP Reactor may also provide a means for accessing the Quantum Gravity (QG) domain for verification or invalidation of various proposed theories by probing for any spacetime curvature, gravitational potential and/or frame-dragging effects. With respect to our modified EFE and FOM equations (15)-(19) and Mathematica models (see Figure 26), we find a significant enhancement of

TABLE II. DPF PROPAGATION AND MAGNETIC RECONNECTION TIMES

Parameter	Value	Unit
DPF plasma current length (L)	0.03	m
DPF plasma current layer thickness (δ)	0.03	m
Magnetic B-cusp field (B)	1	T
Deuteron mass (m_d)	3.34×10^{-27}	kg
Plasma ion density (n)	2×10^{23}	m ⁻³
Plasma ion mass density (ρ)	6.68×10^4	kg m ⁻³
Alfven velocity (V_A)	3.45×10^4	m/s
Magnetic reconnection time (T_R)	8.69×10^{-7}	s
Plasmoid velocity (V_{plasmoid})	10^7	m/s
Distance to collision with other plasmoid (D)	0.10	m
Time to collision after passing through B-cusp (T_C)	1.02×10^{-6}	s
Magnetic reconnection to plasmoid collision times (T_R/T_C)	0.85	

TABLE III. DPF PLASMOID PROPAGATION MODE

Diamagnetic Propagation when $nkT/(B^2/2\mu_0) = \beta > 1$		
Parameter	Value	Unit
Initial plasma density (n_i)	2×10^{23}	m ⁻³
Plasma temperature (T)	15	eV
Plasma pressure (nkT)	4.8×10^5	Pa
Cusp magnetic field (B)	1	T
Magnetic pressure ($B^2/2\mu_0$)	3.98×10^5	Pa
Plasma/magnetic pressure (β)	1.2	satisfied

TABLE IV. ION BEAM PROPAGATION MODES

Collective mode of propagation when $nkT/(B^2/2\mu_0) = \beta \ll 1$ and . . .		
Parameter	Value	Unit / Comment
Initial beam density (n_i)	4.1×10^{18}	m ⁻³
Ion thermal (T_i)	1000	eV
Electron thermal (T_e)	500	eV
Ion beam directed energy (E_b)	4.0×10^7	eV
Beam thermal pressure (nkT)	658	Pa
Initial magnetic field (B)	1	T
Magnetic pressure ($B^2/2\mu_0$)	3.98×10^5	Pa
Beam thermal/magnetic pressure condition ($\beta \ll 1$)	1.65×10^{-3}	satisfied
Square root of mass ratio (m_i/m_e) ^{1/2}	60.6	
Deuterium ion mass (m_i)	3.34×10^{-27}	kg
Electron mass (m_e)	9.1×10^{-31}	kg
Beam ion mass density (ρ)	1.37×10^{18}	kg m ⁻³
Alfven velocity (V_A)	7.62×10^6	m/s
Vacuum permittivity (ϵ_0)	8.85×10^{-12}	F/m
Beam dielectric constant (ϵ)	1.37×10^{18}	F/m
Beam relative permittivity (ϵ_R)	1551	
E-field/energy density condition ($\epsilon_R/(m_i/m_e)^{1/2} \gg 1$)	25.6	satisfied
Beam directed flow (V_b)	6.19×10^6	m/s
Beam directed pressure ($nmv^2/2$)	2.63×10^7	Pa
Beam directed/magnetic pressure condition ($\beta \ll 1$)	0.66	marginally satisfied
Ions thermal velocity ($V_{\text{thermal}(ion)}$)	3.1×10^5	m/s
Electrons thermal velocity ($V_{\text{thermal}(e)}$)	1.33×10^7	m/s
Beam radius (R_b)	0.02	m
Beam initial Larmor radius (R_{Lb})	0.13	m
Thermal ion Larmor radius (R_{Li})	0.0065	m
Thermal electron Larmor radius (R_{Le})	7.54×10^{-5}	m
Beam polarized sheath thickness (δ)	4.16×10^{-6}	m
Polarization condition ($\delta/R_b \ll 1$)	0.0002	satisfied
Beamlet condition ($4R_b/R_L < 1$)	12.38	not satisfied (if E-field not shorted)
Plasma frequency (ω_i)	1.89×10^9	rad/s
Ion cyclotron frequency (Ω_i)	4.79×10^7	rad/s
Electron cyclotron frequency (Ω_e)	1.76×10^{11}	rad/s
Virtual anode formation distance (L)	0.002	m
Virtual anode condition ($(R_L/\epsilon)/L \ll 1$)	0.0019	satisfied

TABLE V. REFLEX TRIODE AND BEAM PARAMETERS

Parameter	Value	Unit
Anode length	0.127	m
Ions per unit length	10^{17}	#/m
Number of ions	1.27×10^{16}	#
Length of beam	0.095	m
Radius of beam	0.02	m
Area of beam	0.032	m^2
Volume of beam	0.003	m^3
Density of beam	4.1×10^{18}	m^{-3}
Single ion beam current	1.3×10^5	A
Two ion beams current	2.6×10^5	A
Erected Marx voltage	4.0×10^5	V
Triode impedance	1.57	Ohms
Single IRMG current	2.5×10^5	A
Two IRMGs current	5.0×10^5	A
Ion beam/IRMG efficiency	51.7	%

Parameter	Ion Ring		Unit
	Value	Value	
Final magnetic field	1250	1250	T
Final ring major radius	0.005	2.73×10^{-6}	m
Final ring volume	1.55×10^{-9}	4.6×10^{-16}	m^3
Final ring density	1.64×10^{25}	5.51×10^{31}	m^{-3}
Particle acceleration	1.8×10^{19}	3.3×10^{22}	m/s^2

Parameter	Electron Ring		Unit
	Value	Value	
Final magnetic field	5000	5000	T
Final ring major radius	0.003	3.4×10^{-7}	m
Final ring volume	6.06×10^{-10}	7.20×10^{-18}	m^3
Final ring density	4.19×10^{25}	1.14×10^{36}	m^{-3}
Particle acceleration	2.87×10^{19}	2.64×10^{23}	m/s^2

energy-momentum to spacetime curvature coupling due to plasma metamaterial effects via the Sarfatti “S” field factor; the initiation of direct spacetime metric phase change generated by accelerating and imploding RHED charged particle rings beyond Unruh/Casimir thresholds via the Anderson “A” field factor and QG effects via Sutherland’s NQG theory with predicted major results provided in Table IX.

IX. CONCLUSION

In conclusion, we envision the WARP Reactor as a more compact, modular and economically viable magneto-inertial fusion device for energy production (i.e. $G > 19/\text{pulse}$, $nT\tau \sim 5.2 \times 10^{21}$ keVs/ m^3) or advanced propulsion and/or a super-radiant flash x-ray/neutron source for dynamic radiographic applications (i.e. x-ray/neutron yields per pulse $> 3.5 \text{MJ}/6.6 \times 10^{18}$, Avg. Luminance $\sim 10^{25}$ x-ray photons / $s \text{mm}^2 \text{mrad}^2$) along with providing access to new relativistic high energy density physics regimes (i.e. multi-MA, GeV-level charged plasma/particle beam-target interactions at multi-TPa, Unruh, Dynamic Casimir & QG effects). The WARP devices would fulfill the immediate need for an intermediate-level machine for z-pinch, beam and pulsed-power flow studies along with the added benefit of recruiting the next-generation of

TABLE VI. RING COMPRESSION AND ACCELERATION METRICS

Parameter	Value	Unit
Speed of light in vacuum	299939418	m/s
Elementary charge	1.6×10^{-19}	C
Proton mass	1.67×10^{-27}	kg
Deuteron mass	3.34×10^{-27}	kg
Triton mass	5.01×10^{-27}	kg
Initial ring energy	10^6	eV
Final ring energy	3.9×10^9	eV
Final to initial ring energy	3906.25	
Initial ring radius	0.25	m
Final ring radius	0.004	m
Initial to final ring radius	62.5	
Initial magnetic field	1	T
Final magnetic field	3906.25	T
Final to initial magnetic field	3906.25	
Proton initial velocity	13848418	m/s
Deuteron initial velocity	9792310	m/s
Triton initial velocity	7995387	m/s
Initial proton Lorentz factor	1.00106	
Initial deuteron Lorentz factor	1.00053	
Initial triton Lorentz factor	1.00035	
Final proton Lorentz factor	5.16	
Final deuteron Lorentz factor	3.08	
Final triton Lorentz factor	2.38	
Proton final azimuthal velocity	291144639	m/s
Deuteron final azimuthal velocity	263001597	m/s
Triton final azimuthal velocity	207792135	m/s
Proton ring final Larmor radius	0.00401	m
Deuteron ring final Larmor radius	0.00433	m
Triton ring final Larmor radius	0.00397	m
Proton ring final azimuthal energy	3.9×10^9	eV
Deuteron ring final azimuthal energy	3.9×10^9	eV
Triton ring final azimuthal energy	3.9×10^9	eV

RHED plasma and accelerator scientists, engineers and technicians. Finally, WARP would be an ideal platform for prototyping novel pulsed power architectures for continuous rep-rate nuclear fusion and radiographic movie operations thereby enabling us to continue our collaborations across the Department of Energy (DOE)/Department of Defense (DOD) complexes along with forging new university and private industry partners through our Cooperative Research and Development Agreement (CRADA) and Strategic Partnership (SPP) programs.

We leave you with the following Gedankenexperiment we call “A Twisted Compression of the Ehrenfest Paradox” along with three conjectures on how one might enhance energy-momentum to spacetime curvature coupling. Imagine you are one of a multitude of elementary charged particles which make up a rotating high-energy-density charge/current neutralized particle ring, embedded within an axial seed magnetic field, that is radially compressed toward zero radius and azimuthally accelerated to ultra-relativistic velocity during sufficient flux compression. According to you and a nearby inertial observer, what happens to the local spacetime surrounding said ring-vortex at the end of the implosion phase?

TABLE VII. FUSION AND RADIATION METRICS FOR DT OPERATIONS

Parameter	Value	Unit
Total machine energy stored (E_0)	10^7	J
Final magnetic field (B_f)	5000	T
Final plasma temperature (T_f)	50000	eV
Confinement time (τ)	10^{-7}	s
Final plasma density (n_f)	1.04×10^{27}	m^{-3}
Final plasma volume (Vol_f)	7.85×10^{-8}	m^3
Number of ions (N)	8.13×10^{19}	#
Average ion velocity ($\langle v \rangle$)	1.96×10^6	m/s
DT fusion cross section ($\langle \sigma \rangle_{DT}$)	4.0×10^{-28}	m^2
DT reaction rate ($\langle \sigma v \rangle_{DT}$)	7.83×10^{-22}	m^3/s
# of fusion neutrons per pulse (N_n)	6.6×10^{18}	#/pulse
Bremsstrahlung energy per pulse (E_{brem})	3.18×10^4	J/pulse
Synchrotron energy per pulse (E_{sync})	3.21×10^6	J/pulse
Fusion energy per pulse (E_f)	1.86×10^7	J/pulse
Plasma energy per pulse (E_p)	9.77×10^5	J/pulse
Scientific gain (E_f/E_p)	19	fraction
Energy for sale (E_{sale})	7.17×10^6	J/pulse
Fusion double product ($n\tau$)	1.04×10^{20}	s/m^3
Fusion triple product ($nT\tau$)	5.18×10^{21}	keV s/m ³
$n\tau/Lawson_{DT}$	0.69	
$nT\tau/LawsonTriple_{DT}$	1.73	

TABLE VIII. RELATIVISTIC HIGH ENERGY DENSITY METRICS

Parameter	DPF Plasma Liner		Unit
	Value	Value	
Final plasma density (n)	10^{27}		m^{-3}
Plasma temperature (T)	50000		eV
Final plasma pressure (nkT)	8.0×10^{12}		Pa
Final magnetic field (B)	5000		T
Magnetic pressure ($B^2/2\mu_0$)	9.95×10^{12}		Pa
Plasma/magnetic pressure (β)	0.8		

Parameter	Ion Ring	e-Ring	Unit
	Value	Value	
Final magnetic field	5000	5000	T
Final ring major radius	0.003	3.4×10^{-7}	m
Final ring volume	6.06×10^{-10}	7.20×10^{-18}	m^3
Final ring density	4.19×10^{25}	1.14×10^{36}	m^{-3}
Particle acceleration	2.87×10^{19}	2.64×10^{23}	m/s^2

```

μp = 1; (*plasma relative permeability [dimensionless]*)
ωp = sqrt((n q^2)/(ε0 me)); (*plasma frequency [rad/s]*)
ω = 2π/Tpulse; (*EM pulse drive frequency [rad/s]*)
εp = 1 + ωp^2/ω^2; (*plasma relative permittivity*)
ar = (ae/ab)^2; (*electron ring relative acceleration to Unruh effect threshold [dimensionless]*)
Rr = (Rering/R0)^3; (*electron ring relative radius to Casimir effect threshold [dimensionless]*)
Sfield = 1/2 * (εp^2 + 1/μp^2); (*Sarfatti S-field [dimensionless]*)
Afield = (ar/Rr)^2; (*Anderson A-field [dimensionless]*)
σGuv = (8πG/c^4) * Sfield Tuv; (*Sarfatti-only spacetime curvature [m^-2]*)
σGuv = (8πG/c^4) * Afield Tuv; (*Anderson-only spacetime curvature [m^-2]*)
σσGuv = (8πG/c^4) * (Afield * Sfield) Tuv; (*Anderson-Sarfatti spacetime curvature [m^-2]*)
Caa = (Afield * Sfield) * (GMring/c^2 Vring); (*Anderson-Sarfatti spacetime curvature approximation [m^-2]*)
φaa = (Afield * Sfield) * (GMring/c^2 Rring); (*Anderson-Sarfatti gravitational potential approximation [dimensionless]*)
ωaa = (Afield * Sfield) * ((G I r ωr)/(c^2 Rr^4));
(*Figure of Merit: Anderson-Sarfatti Lense-Thirring internal angular velocity of inertial dragging field [rad/s]*)

```

Fig. 26. Mathematica models for proposed modified EFE and FOM with Sarfatti and Anderson fields

TABLE IX. METRIC ENGINEERING

Parameter	Value	Unit
Particle density (n_e)	1.04×10^{27}	m^{-3}
Elementary charge (q)	1.6×10^{-19}	C
Electron mass (m_e)	9.1×10^{-31}	kg
Plasma frequency (ω_{pe})	1.82×10^{15}	rad/s
proton mass (m_p)	1.67×10^{-27}	kg
EM-pulse drive frequency ($\omega = 2\pi/T$)	1.57×10^7	rad/s
Non-magnetized plasma relative permittivity (ϵ_r)	-1.35×10^{16}	
Magnetized plasma relative permittivity (ϵ_{rm})	7910	
Spacetime curvature coupling in vacuum ($8\pi G/c^4$)	2.07×10^{-43}	1/N
Plasma refractive index (n)	1.16×10^8	
Sarfatti scalar field factor (S)	9.085×10^{31}	
Anderson scalar field factor (A)	1.9×10^{30}	
Einstein tensor to stress-energy tensor ($G_{\mu\nu}/T_{\mu\nu}$)	1.89×10^{-11}	1/N
Energy-momentum tensor --> energy density ($T_{\mu\nu}$)	1.57×10^{17}	N/m ²
Einstein tensor --> spacetime curvature ($G_{\mu\nu}$)	2.97×10^6	1/m ²
Reciprocal of Einstein tensor ($1/G_{\mu\nu}$)	3.37×10^{-7}	m^2
Final area of particle ring (A_{ring})	1.23×10^{-6}	m^2
Figure of merit for spacetime curvature (C_{aa})	8.64×10^4	1/m ²
Figure of merit for gravitational energy (ϕ_{aa})	3.35×10^{-3}	
Figure of merit for frame-dragging effect (Ω_{aa})	2.3×10^{10}	rad/s
Warp factor ($A_{ring}/(1/G_{\mu\nu})$)	3.66	

Finally, the three possible methods for enhancing energy-momentum to spacetime curvature coupling are as follows:

1. Multi-layer RHED plasma and charged particle ring confinement of THz radiation to create plasma/ring metamaterial effects.
2. Azimuthal acceleration beyond Unruh threshold of multi-pass RHED plasma and charged particle rings to generate Leidenfrost-like vortex layers which create spacetime phase transition.

3. Implosion beyond Casimir threshold of RHED plasma and charged particle rings to generate internal negative energy density which also provides additional confinement mechanism to the $>5\text{kT}$ magnetic fields in order to prevent plasma/ring metamaterial rapid disassembly.

ACKNOWLEDGMENT

The authors would very much like to thank Keith LeChien, Stephen Sampayan and Nathan Meezan for collaboration, reviews, critical discussions and support. This work was performed under the auspices of the U.S. Department of Energy by Lawrence Livermore National Laboratory under Contract DE-AC52-07NA27344.

REFERENCES

- [1] Michael Gordon Anderson, Pulsed Power-Driven Radiation Source System And Method Using A Wave Accelerated Ring Pinch: The WARP Reactor. United States Patent Application #63/499,928, May 3, 2023.
- [2] M. G. Anderson, J. K. Walters, E. M. Anaya and D. A. Max, "Wave Accelerated Ring Pinch eXperiment (WARP-X)," ZNetUS Conference, April 21-22 (2022). <https://znetus.eng.ucsd.edu/home/znetus-workshop>
- [3] W.A. Stygar, et al., "Conceptual designs of two petawatt-class pulsed-power accelerators for high-energy-density-physics experiments," Physical Review, Accel & Beams, V18, 1-30, (2015). <https://doi.org/10.1103/PhysRevSTAB.18.110401>
- [4] P. F. Schmit and D. E. Ruiz, "A conservative approach to scaling magneto-inertial fusion concepts to larger pulsed-power drivers," Physics of Plasmas 27, 062707 (2020). <https://doi.org/10.1063/1.5135716>
- [5] James H. Hammer, Max Tabak, Scott C. Wilks, John D. Lindl, David S. Bailey, Peter W. Rambo, Arthur Toor, and George B. Zimmerman, "High yield inertial confinement fusion target design for a z-pinch-driven hohlraum," Physics of Plasmas 6, 2129 (1999). <https://doi.org/10.1063/1.873464>
- [6] Alcubierre, Miguel "The Warp Drive: Hyper-fast Travel Within General Relativity," Classical and Quantum Gravity 11 (1994). <https://doi.org/10.1088/0264-9381/11/5/001>
- [7] Erik W Lentz, "Breaking the warp barrier: hyper-fast solitons in Einstein–Maxwell-plasma theory," Classical and Quantum Gravity 38 075015 (2021). <https://doi.org/10.1088/1361-6382/abe692>
- [8] Glenn, Chance, "Positive Energy Density for the Alcubierre Warp Field Equations Using an RF-Driven Dielectric Resonant Cavity," TechRxiv. Preprint. <https://doi.org/10.36227/techrxiv.19224552.v1>
- [9] Harold G. White, "A Discussion of Space-Time Metric Engineering," General Relativity and Gravitation, Vol. 35, No. 11, November (2003). <https://doi.org/10.1023/A:1026247026218>
- [10] H. G. White and E. W. Davis, "The Alcubierre Warp Drive in Higher Dimensional Spacetime," AIP Conference Proceedings 813, 1382 (2006). <https://doi.org/10.1063/1.2169323>
- [11] White, Harold "Warp Field Mechanics 101," 100 Year Starship Symposium DARPA/NASA JSC-CN-24651 September 30 (2011). <https://ntrs.nasa.gov/citations/20110015936>
- [12] André Füzfa, "How current loops and solenoids curve spacetime," Phys. Rev. D 93, 024014 – Published 11 January (2016). <https://doi.org/10.1103/PhysRevD.93.024014>
- [13] Bailey, J., Borer, K., Combley, F. et al. "Measurements of relativistic time dilatation for positive and negative muons in a circular orbit," Nature 268, 301–305 (1977). <https://doi.org/10.1038/268301a0>
- [14] Alexey Bobrick and Gianni Martire, "Introducing physical warp drives," Classical and Quantum Gravity 38 105009 (2021). <https://doi.org/10.1088/1361-6382/abd6fc>
- [15] H. E. Puthoff, "Can the Vacuum Be Engineered for Spaceflight Applications? Overview of Theory and Experiments," Journal of Scientific Exploration, Vol. 12 No. 1, pp. 295-302, (1998). <http://www.zamandayolculuk.com/pdf-1/vacuumengineered-pdf>
- [16] Puthoff, H.E. "Casimir Vacuum Energy and the Semiclassical Electron," International Journal of Theoretical Physics 46, 3005–3008 (2007). <https://doi.org/10.1007/s10773-007-9414-2>
- [17] Davis, Eric and Puthoff, Harold. "On Extracting Energy from the Quantum Vacuum," AIAA ResearchGate August (2019). <https://www.researchgate.net/publication/335432514>
- [18] Rodrigo Medina, J. Stephany, "The energy-momentum tensor of electromagnetic fields in matter," Classical Physics arXiv:1703.02109 [physics.class-ph] (2017). <https://doi.org/10.48550/arXiv.1703.02109>
- [19] Millette, Pierre "On the Question of Acceleration in Special Relativity," Progress in Physics 1555-5534. 13. 213-217 (2017). <https://www.researchgate.net/publication/321049014>
- [20] Barbara Šoda, Vivishek Sudhir, and Achim Kempf, "Acceleration-Induced Effects in Stimulated Light-Matter Interactions," Phys. Rev. Lett. 128, 163603 – Published 21 April (2022). <https://doi.org/10.1103/PhysRevLett.128.163603>
- [21] Guido Rizzi and Matteo Luca Ruggiero, "Space Geometry of Rotating Platforms: An Operational Approach," Foundations of Physics, Vol. 32, No. 10, October (2002). <https://doi.org/10.1023/A:1020427318877>
- [22] S. Al Saleh*, L. A. Al Asfar, A. Mahroussah, "Rotating Squeezed Vacua as Time Machines," Journal of Modern Physics > Vol.7 No.3, February (2016). <http://dx.doi.org/10.4236/jmp.2016.73030>
- [23] Abellán, G., Bolivar, N. & Vasilev, I. "Alcubierre warp drive in spherical coordinates with some matter configurations," Eur. Phys. J. C 83, 7 (2023). <https://doi.org/10.1140/epjc/s10052-022-11091-5>
- [24] Pierre A. Millette, "On Time Dilation, Space Contraction, and the Question of Relativistic Mass," PROGRESS IN PHYSICS Volume 13 Issue 4 (2017). <https://www.researchgate.net/publication/321048772>
- [25] A. Schmidt, E. Anaya, M. Anderson, J. Angus, S. Chapman, C. Cooper, O. Drury, C. Goyon, S. Hawkins, D. P. Higginson, I. Holod, E. Koh, A. Link, D. Max, M. McMahon, J. Mitrani, Y. Podpaly, A. Povilus, and D. Van Lue, "First Experiments and Radiographs on the MegaJoule Neutron Imaging Radiography (MJOLNIR) Dense Plasma Focus," IEEE Transactions on Plasma Science, (49) 3299 (2021). <https://doi.org/10.1109/TPS.2021.3106313>
- [26] J.H. Lee, et al. "Dense plasma focus production in a hypocycloidal pinch," NASA-TN-D-8116 L-10549 Report (1975). <https://ntrs.nasa.gov/citations/19760007844>
- [27] Ja H. Lee, Donald R. McFarland, and Frank Hohl, "Production of dense plasmas in a hypocycloidal pinch apparatus," The Physics of Fluids 20, 313 (1977). <https://doi.org/10.1063/1.861869>
- [28] B. V. Weber et al., "Reflex triode x-ray source research on Gamble II," 2007 16th IEEE International Pulsed Power Conference, Albuquerque, NM, USA, pp. 1417-1422, (2007). <https://doi.org/10.1109/PPPS.2007.4652453>
- [29] Jack Sarfatti, "Lectures in Metric Engineering Physics," Academia, August 4, (2022). <https://www.academia.edu/83953289>
- [30] Roderick Sutherland, "Naive Quantum Gravity," General Relativity and Quantum Cosmology (gr-qc); Quantum Physics (quant-ph), (2019). <https://doi.org/10.48550/arXiv.1502.02058>
- [31] Vitaly Bystritskii, Frank J. Wessel, Norman Rostoker, Hafiz Rahman, "Novel Staged Z-Pinch Concept as Super Radiant X-Ray Source for ICF," Current Trends in International Fusion Research pp 347-364, (1997). https://doi.org/10.1007/978-1-4615-5867-5_22
- [32] J.B. Greenly, "Ion Rings for Magnetic Fusion," Technical Report, DOE/ER/54221-F, TRN: US1002814 (2005). <https://doi.org/10.2172/862052>
- [33] Norman Rostoker, Michl Binderbauer, Frank Wessel, Alex Cheung, Vitaly Bystritskii, Yuanxu Song, Michael Anderson, Eusebio Garate, Alan Vandrie, "Plasma Electric Generation System. European Patent Number: EP1856702B1, Granted: 2012-07-18. <https://patentimages.storage.googleapis.com/b5/f5/3c/934301bc437e31/EP1856702B1.pdf>
- [34] R. J. Faehl and G. Gisler, "Intense Ion Ring Acceleration in a Flux Compressing Liner," in IEEE Transactions on Nuclear Science, vol. 30, no. 4, pp. 3201-3203, Aug. (1983). <https://doi.org/10.1109/TNS.1983.4336614>

- [35] Kapetanacos, C. A. "Generation of intense, high-energy ion pulses by magnetic compression of ion rings". United States. US 4293794 (1981). <https://www.osti.gov/biblio/5754088>
- [36] R. N. Sudan and P. M. Lyster, "A study of the magnetic compression of energetic ion layers in conductive plasmas," *Physics of Plasmas* 1, 1783-1791 (1994). <https://doi.org/10.1063/1.870685>
- [37] R. N. Sudan, "Ion-Ring Igniter for Inertial Fusion," *Physical Review Letters* 41, 476 – August (1978). <https://doi.org/10.1103/PhysRevLett.41.476>
- [38] M. Reiser, *Theory and Design of Charged Particle Beams*, Wiley, Weinheim, Germany (2008). <https://doi.org/10.1002/9783527622047>
- [39] S. Dzarakhokhova, N. P. Zaretskiy, A. V. Maksimych, L. I. Men'shikov & P. L. Men'shikov, "Acceleration of Ion Rings by Collapsing Liners," *Technical Physics*, Vol. 65, No. 6, pp. 865–873. (2020). <https://doi.org/10.1134/S1063784220060092>
- [40] S. Dzarakhokhova, N. P. Zaretskiy, A. V. Maksimych, L. I. Men'shikov & P. L. Men'shikov, "Conditions For The Stable Acceleration of Ion Rings by Collapsed Liners" *Journal of Experimental and Theoretical Physics*, Vol. 130, No. 1, pp. 140–147 (2020). <https://doi.org/10.1134/S1063776120010021>
- [41] Ribe, F L, Oliphant, Jr, T A, and Quinn, W E. "FEASIBILITY STUDY OF A PULSED THERMONUCLEAR REACTOR," LASL Report LA-3294 United States (1965). <https://www.osti.gov/biblio/4613663>
- [42] D.J. Rose, "Engineering feasibility of controlled fusion: A Review," *Nuclear Fusion*, Volume 9, Number 3 183 (1969). <https://doi.org/10.1088/0029-5515/9/3/001>
- [43] S Yu Gus'kov and Yu K Kurilenkov, "Neutron yield and Lawson criterion for plasma with inertial electrostatic confinement," *Journal of Physics: Conference Series* 774 012132 (2016). <https://doi.org/10.1088/1742-6596/774/1/012132>
- [44] S. Lee et al., "Numerical experiments on plasma focus neutron yield versus pressure compared with laboratory experiments," *Plasma Physics and Controlled Fusion* 51 075006 (2009). <https://doi.org/10.1088/0741-3335/51/7/075006>
- [45] J. Narkis, H. U. Rahman, J. C. Valenzuela, et al., "A semi-analytic model of gas-puff liner-on target magneto-inertial fusion," *Physics of Plasmas* 26, 032708 (2019). <https://doi.org/10.1063/1.5086056>
- [46] Igor I. Smolyaninov, "Metamaterial-based model of the Alcubierre warp drive," *Physical Review B* 84, 113103 September (2011). <https://doi.org/10.1103/PhysRevB.84.113103>
- [47] Osamu Sakai and Kunihide Tachibana, "Plasmas as metamaterials: a review," *Plasma Sources Science and Technology*, Volume 21, Number 1 013001 (2012). <https://doi.org/10.1088/0963-0252/21/1/013001>
- [48] Anderson, O.A., Baker, W.R., Bratenahl, A., Ise, J. Jr., Kunkel, W.B., Stone, J.M., & Furth, H.P. "Study and use of rotating plasma" (INIS-XU-022). United Nations (1958). <https://inis.iaea.org/search/39084591>
- [49] Oscar Anderson, William R. Baker, Alexander Bratenahl, Harold P. Furth, and Wulf B. Kunkel, "Hydromagnetic Capacitor," *Journal of Applied Physics* 30, 188 (1959). <https://doi.org/10.1063/1.1735132>
- [50] W. A. Stygar, K. R. LeChien, et al., "Impedance-matched Marx generators," *Physical Review Accelerator and Beams* Volume 20, 040402 – April (2017). <https://doi.org/10.1103/PhysRevAccelBeams.20.040402>
- [51] Leckbee, Joshua, Oliver, Bryan V, Toury, Martial, Cartier, Frederic, and Caron, Michel "Two pulses tests with a single LTD cavity," Sandia National Lab Report SAND2012-9031C United States (2012). <https://www.osti.gov/biblio/1062277>
- [52] B. N. Turman, T. H. Martin, E. L. Neau, D. R. Humphreys, D. D. Bloomquist, D. L. Cook, S. A. Goldstein, L. X. Schneider, D. H. McDaniel, J. M. Wilson, R. A. Hamil, G. W. Barr, and J. P. VanDevender, "PBFA II: A 100 TW Pulsed Power Driver for the Inertial Confinement Fusion Program," Sandia National Lab Report, June (1985). <https://apps.dtic.mil/sti/pdfs/ADA638630.pdf>
- [53] T. H. Martin, B. N. Turman, S. A. Goldstein, J. M. Wilson, D. L. Cook D. H. McDaniel, E. L. Burgess, G. E. Rochau, E. L. Neau and D. R. Humphreys "PBFA II, The Pulsed Power Characterization Phase," Sandia National Lab Report June (1987). <https://apps.dtic.mil/sti/pdfs/ADA638733.pdf>
- [54] Ryan D. McBride and Stephen A. Slutz, "A semi-analytic model of magnetized liner inertial fusion," *Physics of Plasmas* 22, 052708 (2015). <https://doi.org/10.1063/1.4918953>
- [55] R. D. McBride, S. A. Slutz, R. A. Vesey, M. R. Gomez, A. B. Sefkow, S. B. Hansen, P. F. Knapp, P. F. Schmit, M. Geissel, A. J. Harvey-Thompson, C. A. Jennings, E. C. Harding, T. J. Awe, D. C. Rovang, K. D. Hahn, M. R. Martin, K. R. Cochran, K. J. Peterson, G. A. Rochau, J. L. Porter, W. A. Stygar, E. M. Campbell, C. W. Nakhleh, M. C. Herrmann, M. E. Cuneo, and D. B. Sinars, "Exploring magnetized liner inertial fusion with a semi-analytic model", *Physics of Plasmas* 23, 012705 (2016). <https://doi.org/10.1063/1.4939479>
- [56] P. Kubes, et al. "Scenario of a magnetic dynamo and magnetic reconnection in a plasma focus discharge," *Matter and Radiation at Extremes* 5, 046401 (2020). <https://doi.org/10.1063/1.5133103>
- [57] J.D. Hare, et al., "An experimental platform for pulsed-power driven magnetic reconnection," *Physics of Plasmas* 25, 055703 (2018). <https://doi.org/10.1063/1.5016280>
- [58] M. Anderson, et al., "Propagation of intense plasma and ion beams across B-field in vacuum and magnetized plasma," *Laser and Particle Beams*, vol.23 pp.117-129, Cambridge University Press, (2005). <https://doi.org/10.1017/S0263034605050202>
- [59] M.G. Anderson "Formation and Propagation of Pulsed High Current Plasma and Ion Beams in Transverse Magnetic Field and Magnetized Plasma," and "The Development of High Current Accelerators in the United States of America," PhD Dissertation (2006).
- [60] M. W. Binderbauer, H. Y. Guo, M. Tuszewski, N. Rostoker, M. G. Anderson, et al., "Dynamic Formation of a Hot Field Reversed Configuration with Improved Confinement by Supersonic Merging of Two Colliding High-beta Compact Toroids" *Physical Review Letters*, vol.105, pp. 045003, (2010). <https://doi.org/10.1103/PhysRevLett.105.045003>
- [61] M. Anderson, V. Bystritskii, and J. K. Walters, "Double and multi-pulsed operations of inductive plasma sources," *Nuclear Instruments and Methods A*, vol.545, pp.578-592, Elsevier Press. (2005). <https://doi.org/10.1016/j.nima.2005.02.030>
- [62] M. Anderson, M. Binderbauer, V. Bystritskii, E. Garate, N. Rostoker, Y. Song, A. Van Drie, and I. Isakov. Plasma and Ion Beam Injection into an FRC. *Plasma Physics Reports*, vol.31, no.10, pp.809-817, (2005). <https://link.springer.com/content/pdf/10.1134/1.2101968.pdf>
- [63] Michael Anderson, Vitaly Bystritskii, Kurt Walters, et al., "Colliding Tori Fusion Reactor," IEEE International Power Modulator and High Voltage Conference in San Diego, CA June 3 - 7 (2012). <https://www.nessengr.com/ipmhvc2012>